2018

Performance Analysis of Active Magnetic Regenerative Refrigeration Cycle using Transient Modeling

Minwoong Kang
UIUC, United States of America, mk16@illinois.edu

Stefan Elbel
elbel@illinois.edu

Performance Analysis of Active Magnetic Regenerative Refrigeration Cycle using Transient Modeling

Minwoong Kang[1], Stefan Elbel[1,2,*]

[1] Air Conditioning and Refrigeration Center, Department of Mechanical Science and Engineering, University of Illinois at Urbana-Champaign, 1206 West Green Street, Urbana, IL 61801, USA
[2] Creative Thermal Solutions, Inc., 2209 North Willow Road, Urbana, IL 61802, USA
* Corresponding Author
Email: elbel@illinois.edu

ABSTRACT

This paper evaluates the performance of an active magnetic regenerative refrigeration cycle (AMRRC) by using transient modeling tools. While theoretical COPs of magnetic refrigeration systems are quite promising, parasitic losses inherent to the cycle can substantially reduce the energy efficiency that can be achieved in reality. For solid state refrigeration systems, such as the AMRR cycle, the regenerator undergoes cyclic heating and cooling, making the thermal capacitance of the component a critical parameter during no flow periods. Additional performance reductions are experienced due to additional temperature differences required to convect heat into and out of the magnetic regenerator through the use of a secondary heat transfer fluid. Therefore, this paper combines transient modeling of the magnetic regenerator and the heat exchangers that connect the system to the heat source and sink. The model is then used to study the effects of relevant parameter variations, including magnetic cycling and fluid flow frequencies, mass flow rate of the secondary fluid stream, and geometric variations of the regenerator design, on parasitic losses, cooling capacity and COP. In addition, the model is used to assess the COP reduction caused by these inherent parasitic losses, which allow for a fairer comparison to standard vapor compression systems.

1. INTRODUCTION

Magnetic refrigeration cycle is seen as one of the most promising technologies to replace the conventional vapor compression cycle (VCC). It has been actively investigated because of its environmental-friendly characteristics. Not having to us a refrigerant is considered another advantage of the technology, eliminating the problem direct greenhouse gas emissions and problems caused through refrigerant leakage. Furthermore, the inherently high energy efficiency of the AMRR cycle makes this technology an attractive candidate for future cooling systems. Because of these advantages, magnetic refrigeration cycle has been emphasized as alternative with the best experimentally achieved exergetic efficiency among different cooling and heating technologies (Brown and Domanski, 2014).

Magnetic refrigeration cycles generate cooling and heating utilizing the magnetocaloric effect which is the physical phenomenon of magnetocaloric material (MCM) exposed to a magnetic field change. When a magnetic field is applied to an MCM, which is called the magnetization process, the magnetic entropy of the MCM decreases. In isentropic condition an increase in lattice entropy due to constant total entropy causes an increase in temperature of the material which is called adiabatic temperature change of magnetization. When the magnetic field is removed from the material, its temperature decreases. This cyclic magnetocaloric effect can be used for cooling and heating in a magnetic refrigeration cycle (Kitanovski, 2015).

However, a maximum adiabatic temperature change of most MCMs using a permanent magnet cannot exceed 5K, which is insufficient to replace conventional VCCs which can deliver much more substantial temperature lifts. Therefore, an active magnetic regenerative refrigeration cycle (AMRRC) was developed and applied to magnetic refrigeration cycle by Steyert (1978) and Barclay and Steyert (1982) to increase obtainable temperature lifts. A higher temperature lift is achieved, by connecting the MCM via heat transfer fluid (HTF) to the heat source and the heat sink in an alternating fashion. A typical AMRRC consists of the four processes described in Figure 1. It continuously repeats and Kitanovski (2015) compared its cyclic operation to the characteristics of a Brayton cycle.

(a) Magnetization: when magnetic field applied in MCM, the MCM temperature increases
(b) Fluid flow from cold to hot: when HTF passes from cold to hot side of regenerator heat is transferred from MCM to HTF and temperature of MCM decreases
(c) Demagnetization: when magnetic field is removed from MCM, its temperature decreases

(d) Fluid flow from hot to cold: when HTF passes from hot to cold side of the regenerator heat is transferred from HTF to MCM and the temperature of the MCM increases

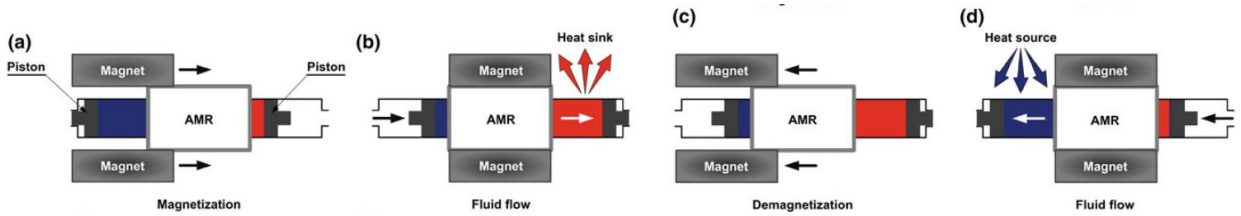

Figure 1: Schematics of the four basic operational phases of the AMRRC (Kitanovski, 2015)

Numerous thermodynamic models for AMRRC have been developed. Most of these models focus on steady-state conditions, and are concerned with optimum regenerator design. Consequently, heat transfer between MCM and HTF during no flow periods is neglected. 1D porous and parallel plate regenerator models have been used to investigate the effect of HTF mass flow rate, as well as rotational frequency and volume of regenerator on the performance of the magnetic refrigeration cycle (Engelbrecht, 2004). 1D and 2D models are compared by Petersen *et al.* (2013). Their paper concluded that although a 1D model can predict overall results, a 2D model is required to study detailed characteristics of the AMRRC. The purpose of this paper is to add to this investigation by comparing thermodynamic models with and without heat transfer during no flow periods, which are considered parasitic losses in magnetic refrigeration cycle. Additional inherent parasitic loss due to temperature differences required to heat or cool the magnetic regenerator and heat transfer fluid during cyclic heating and cooling has been calculated. The tool developed is a transient 1D model which can be used to optimize heat exchangers of AMRRC.

2. NUMERICAL MODEL

Figure 2 shows the schematic of the modeled magnetic refrigeration cycle. The system consists of a rotating regenerator bed, two heat exchangers and a permanent magnet. The regenerator is made of six individual regenerator beds which are filled with spherical MCM through which heat transfer fluid passes. The packed-sphere regenerator is magnetized and demagnetized repeatedly by rotating into and out of a magnetic field caused by a stationary permanent magnet. The performance of this cycle using 2 Tesla of magnetic field is investigated using 1D modeling. Reservoir tanks are added between the regenerator and the heat exchangers to improve numerical stability of the simulation model.

Figure 3 displays the adiabatic temperature change and specific heat capacity during magnetization for gadolinium MCM (Tishin *et al.*, 1999, Aprea *et al.*, 2013). These values serve as modeling inputs through polynomial equations to reduce computational time.

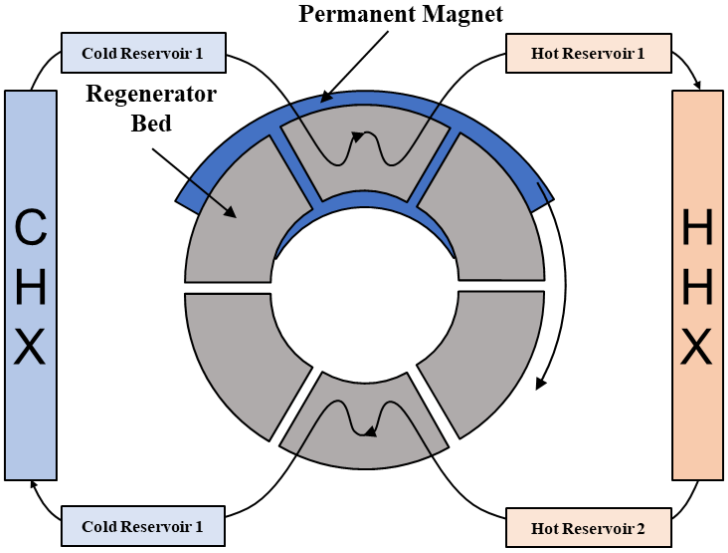

Figure 2: Schematic of modeled magnetic refrigeration cycle

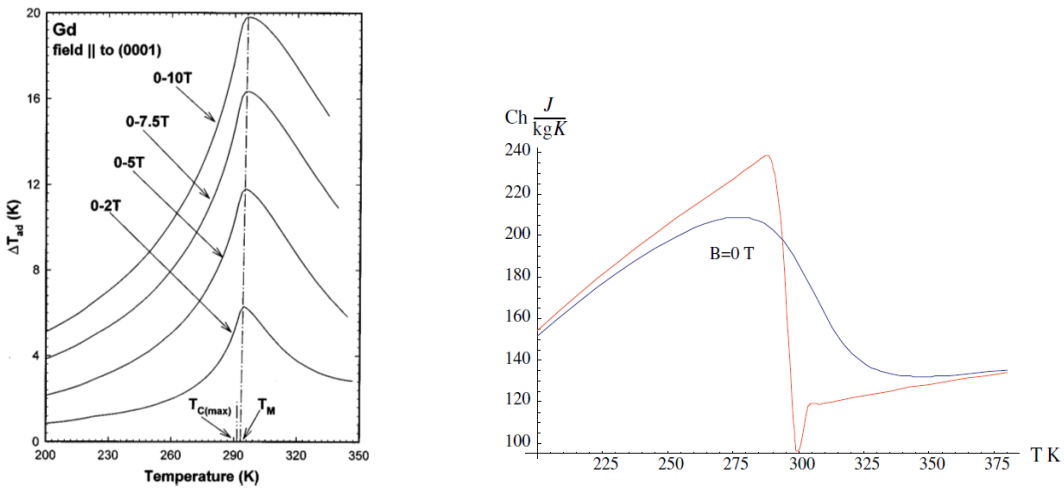

(a) (b)

Figure 3: (a) Adiabatic temperature change during magnetization (Tishin *et al.*, 1999) and (b) specific heat capacity for gadolinium (Aprea *et al.*, 2013)

2.1 Energy balance of regenerator bed

The energy balance of the HTF in the regenerator is shown in Figure 4 and Equation (1).

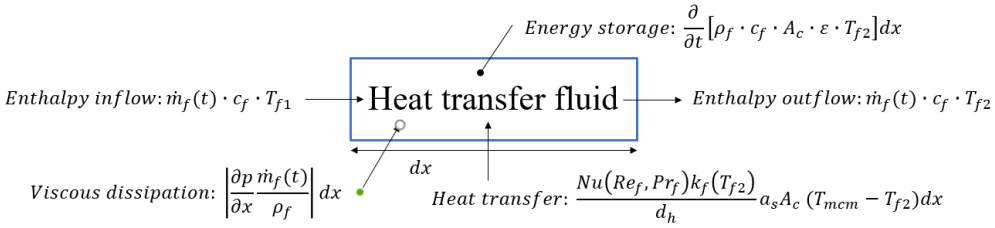

Figure 4: Energy balance of HTF in regenerator

$$\frac{Nu \cdot k_f}{d_h} a_s A_c \left(T_{mcm} - T_{f2}\right)dx = \dot{m}_f \cdot c_f \cdot (T_{f2} - T_{f1}) + m_f \cdot c_f \cdot \frac{dT_{f2}}{dt} - \left|\frac{\partial p}{\partial x}\frac{\dot{m}_f}{\rho_f}\right| dx \quad (1)$$

The energy balance of spherical MCM used in the regenerator is shown in Figure 5 and Equation (2).

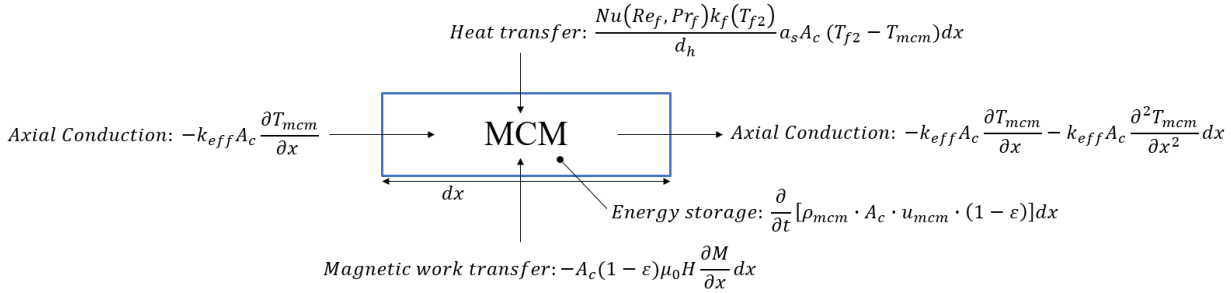

Figure 5: Energy balance of MCM used in regenerator

$$\frac{Nu \cdot k_f}{d_h} a_s A_c \left(T_{f2} - T_{mcm}\right)dx = m_{mcm} \cdot c_{mcm} \cdot \frac{dT_{mcm}}{dt} - k_{eff} A_c \frac{\partial^2 T_{mcm}}{\partial x^2} dx \quad (2)$$

The axial conduction within the HTF is neglected in Equation (1). However, axial conduction is considered in Equation (2) using effective conductivity because of the HTF's high thermal conductivity (Engelbrecht, 2008). The second term on the right side of Equation (1) represents the specific heat capacity of the HTF. This term is used to account for heat transfer between MCM and HTF and the effect of the loss on system performance during no flow periods.

The magnetic work transfer to MCM is not considered in Equation (2). Instead, the magnetic work results in an adiabatic temperature increase of the MCM during magnetization and an adiabatic temperature decrease during demagnetization. These processes are shown in Figure 6.

For magnetization process:

$$T_{mcm,mag,i} = T_{mcm,dem,f} + \Delta T_{mag}(T_{mcm,dem,fi}) \tag{3}$$

For demagnetization process:

$$T_{mcm,dem,i} = T_{mcm,mag,f} + \Delta T_{dem}(T_{mcm,mag,fi}) \tag{4}$$

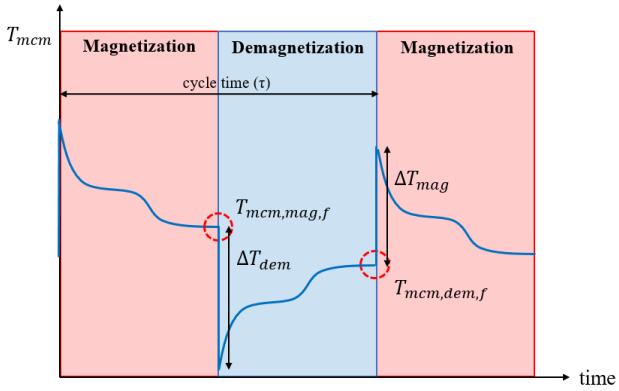

Figure 6: Calculation of magnetic work transfer

2.2 Heat transfer coefficient between MCM & HTF

The Biot number of the regenerator is larger than 0.1, so there is a significant temperature gradient between the center and the outer surface of the MCM. The heat transfer coefficient should be corrected according to Equation (5), because heat conduction in the MCM cannot be neglected (Dixon and Cresswell, 1979). The specific surface area a_s is calculated according to Equation (6) and h* can be calculated using Equation (7) (Dixon & Cresswell, 1979).

$$h = a_s h^* \tag{5}$$

$$a_s = \frac{6(1-\varepsilon)}{D_h} \tag{6}$$

$$\frac{1}{h^*} = \frac{d_h}{Nu_f k_f} + \frac{d_h}{\beta k_s} \tag{7}$$

where β = 10 (spherical shape) and an empirical correlation for the Nusselt number in a packed-sphere bed is used according to Equation (8) (Wakao & Kaguei, 1982)

$$Nu_f = 2.0 + 1.1 Pr^{1/3} Re^{0.6} \tag{8}$$

2.3 Heat exchanger model

Heat exchangers are simulated by the ε-NTU method. As already mentioned, reservoir tanks are located between the regenerator and the heat exchangers for the purpose of improving numerical stability. The reservoir (reservoir 1) located in the downstream part of the regenerator is included in the magnetization calculation process and its temperature varies as time progresses. The final temperature of the reservoir ($T_{res,1}(\tau)$) serves as an input to the post-magnetization process to calculate the heating capacity and the outlet temperature of the heat exchanger (T_{out}) which is constant as shown in Figure 7 (τ is the time period of magnetization).

Outlet temperature of reservoir downstream of heat exchanger ($T_{res,2}(\tau)$) calculated by Equation (9) which is utilized as fluid temperature entering hot side of regenerator for demagnetization process and same process is applied into demagnetization and post-demagnetization process.

$$T_{res2}(\tau) = T_{out} + (T_{res2,\,i} - T_{out}) \times e^{\left(-\frac{\dot{m}}{M}\times\tau\right)} \tag{9}$$

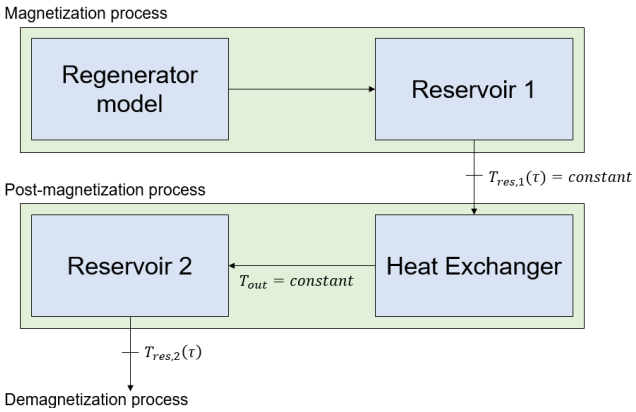

Figure 7: Calculation of temperature of reservoir tanks and heating capacity of heat exchanger

2.4 Coefficient of performance (COP)

COP is calculated using below equation.

$$COP = \frac{\dot{Q}_c}{\dot{W}} \tag{10}$$

Where

$$\dot{Q}_h = \int \dot{m}\, c_p (T_{mcm,outlet} - T_{mcm,inlet}) \tag{11}$$

$$\dot{Q}_c = \int \dot{m}\, c_p (T_{mcm,outlet} - T_{mcm,inlet}) \tag{12}$$

$$\dot{W} = \dot{Q}_h + \dot{Q}_c \tag{13}$$

3. RESULTS AND DISCUSSION

3.1 Convergence along spatial steps

Table 1 shows the system parameters used in the AMRRC model. These parameters are same as Engelbrecht (2008). Table 2 shows COP as a function of the number of spatial steps. It is observed that simulations using more than 40 spatial steps (m) result within 95% of the COP achieved with m=110. Therefore, the simulations carried out for this study generally used 60 spatial steps to both address convergence and computation speed.

Table 1: System parameters for model inputs (Engelbrecht, 2008)

Parameter	Value	Parameter	Value
Maximum applied field	1.5 Tesla	Heat transfer fluid	Water
Cold air flow rate	0.57 kg/s	Fluid mass flow rate	1.4 kg/s
Hot air flow rate	1.42 kg/s	Period	0.2 s (5 Hz)
Cold heat exchanger UA	0.880 kW/K	Sphere size for packing	0.2 mm
Hot heat exchanger UA	1.430 kW/K	Cycle time	0.4 s
Regenerator volume	10 L	Regenerator type	Packed sphere

Table 2: COP as a function of number of spatial steps

Spatial variable (m)	COP	COP/COP_{110} (%)	$\dot{W}_{input}$ (kW)	$\dot{Q}_{cooling}$ (kW)	$\dot{Q}_{heating}$ (kW)	$T_{reservoir,hot}$ (°C)	$T_{reservoir,cold}$ (°C)
40	18.0	95.0	0.88	3.12	6.38	34.4	19.7
50	18.1	95.5	0.92	3.25	6.68	34.8	19.4
60	18.2	96.1	0.94	3.35	6.92	35.1	19.2
70	18.1	95.4	0.97	3.43	7.09	35.3	19.0
80	18.5	97.6	0.97	3.51	7.23	35.5	18.8
90	18.9	99.5	0.97	3.58	7.35	35.6	18.7
100	18.6	98.0	1.00	3.63	7.44	35.7	18.5
110	19.0	-	1.00	3.70	7.50	35.8	18.4

3.2 Time convergence

COP as a function of number of spatial steps is shown in Figure 8. It has been observed that simulations with more than 300 cycles converge to within 95% of the COP achieved with 1000 cycles. Therefore, it is assumed that the model after 300 cycles reaches steady-state, unless otherwise mentioned. For steady-state operation the temperature gradient of the MCM along the length of the regenerator is given in Figure 9. The temperatures of the hot and cold reservoir tanks are 37.5°C and 18.9°C, respectively and the heating and cooling capacities are 8.93kW and 3.48kW, respectively. These results differ slightly from those of Engelbrecht (2008) because of using different values for adiabatic temperature change and specific heat capacity of the MCM and heat capacities of the fluid reservoirs.

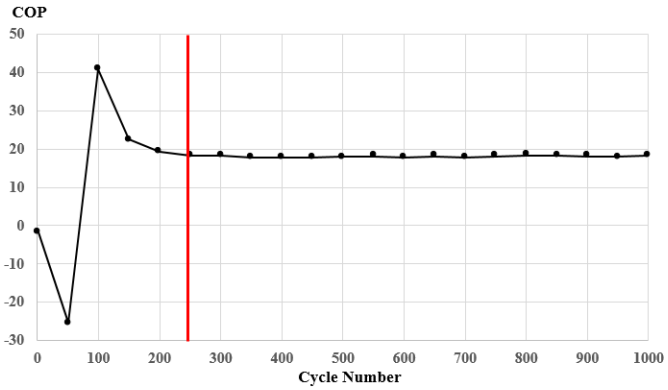

Cycle	COP	COP/COP_{1000} (%)
1	-1.86	-10.19
100	40.91	224.29
200	19.31	105.87
300	18.22	99.89
400	17.83	97.75
500	17.96	98.46
600	17.86	97.92
700	17.86	97.92
800	18.42	100.99
900	18.13	99.40
1000	18.24	100.00

Figure 8: Convergence as a function of number of cycles

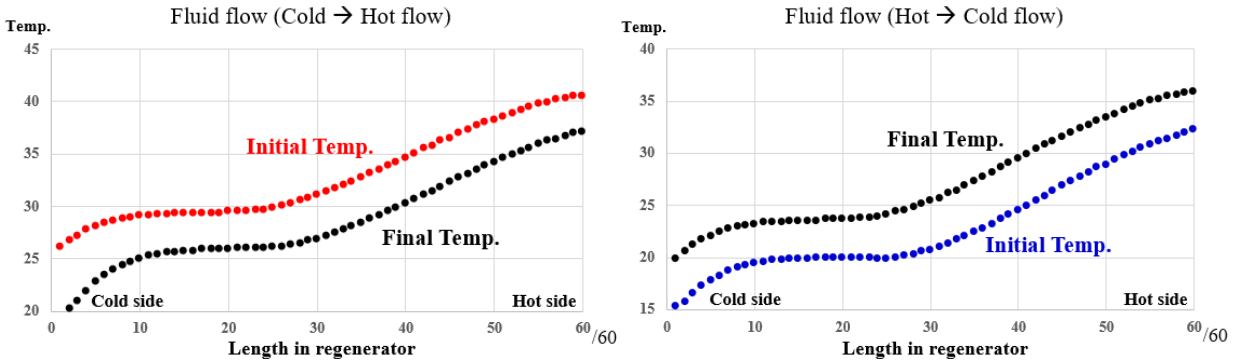

Figure 9: Temperature gradient of the MCM along the length of regenerator

3.3 Comparison of models with and without heat transfer during no flow period

This paper uses the model without heat transfer during no flow period, which is not a real situation in AMRRC but ideal one to simplify the model. The AMRRC in reality includes no flow periods before and after mass flow period in magnetization and demagnetization processes. The model with heat transfer is compared with the model without heat transfer during no flow period. For this comparison, the initial temperature of the MCM is given as having temperature gradient from 25°C on the cold side to 40°C on the hot side. The initial temperature of HTF is given as having temperature gradient from 20°C on the cold side to 35°C on the hot side. The initial temperatures of the hot and cold reservoir tanks are assumed to be 38°C and 18°C, respectively. Temperature change of the hot and cold sides of the MCM and HTF after one cycle are shown in Figure 10 and Table 3. According to this comparison, there is no significant difference between these models. The difference of heat transfer between these models is only 0.2 ~ 0.3 %. This is because the heat transfer between MCM and HTF is very fast, so heat transfer during no flow period cannot make big difference.

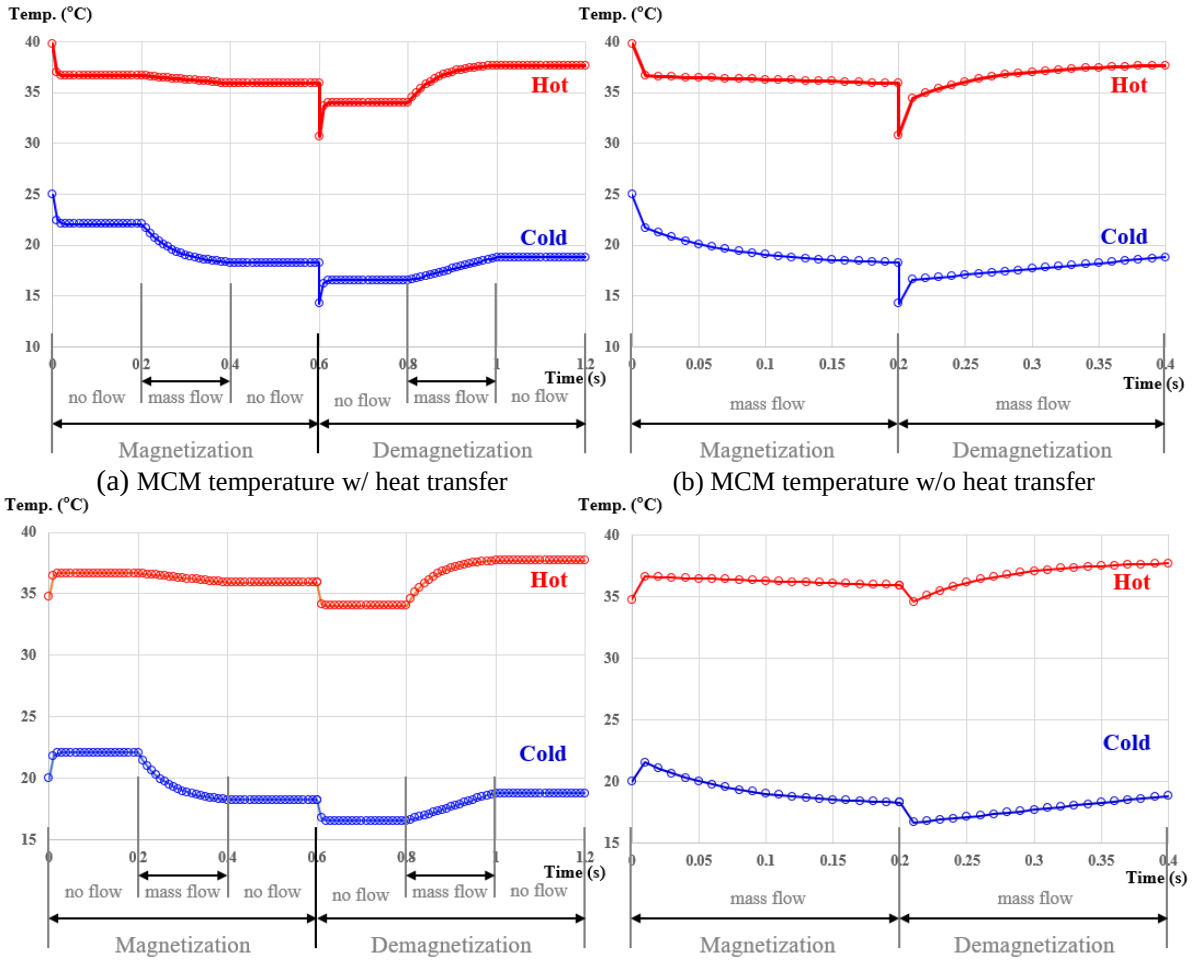

(a) MCM temperature w/ heat transfer (b) MCM temperature w/o heat transfer

(c) HTF temperature w/ heat transfer (d) HTF temperature w/o heat transfer

Figure 10: Temperature change in hot and cold sides of MCM and HTF

Table 3: Temperature changes in hot and cold sides of MCM and HTF

MCM Temp.		**w/ heat transfer**								**w/o heat transfer**			
		Mag.				**Dem.**				**Mag.**		**Dem.**	
Time		0.0	0.2	0.4	0.6	0.6	0.8	1.0	1.2	0.0	0.2	0.2	0.4
Flow		-	No flow	Mass flow	No flow	-	No flow	Mass flow	No flow	-	Mass flow	-	Mass flow
Temp.	Hot	39.75	36.68	35.92	35.91	30.74	34.02	37.69	37.69	39.75	35.92	30.75	37.69
	Cold	25.00	22.11	18.28	18.28	14.24	16.57	18.79	18.81	25.00	18.29	14.25	18.79
HTF Temp.		**w/ heat transfer**								**w/o heat transfer**			
		Mag.				**Dem.**				**Mag.**		**Dem.**	
Time		0.0	0.2	0.4	0.6	0.6	0.8	1.0	1.2	0.0	0.2	0.2	0.4
Flow		-	No flow	Mass flow	No flow	-	No flow	Mass flow	No flow	-	Mass flow	-	Mass flow
Temp.	Hot	34.75	36.68	35.91	35.91	35.91	34.02	37.70	37.69	34.75	35.91	35.91	37.70
	Cold	20.00	22.11	18.27	18.28	18.28	16.57	18.81	18.81	20.00	18.27	18.27	18.82

3.4 Parasitic losses by cyclic heating and cooling

There are inherent parasitic losses due to cyclic heating and cooling in AMRRC. In other words, some energy is required to heat the initially cold MCM and HTF during the magnetization process and to cool the initially hot MCM and HTF during the demagnetization process. These losses are the big difference between these solid-state

refrigeration systems in which the temperature of regenerator beds continuously change and conventional vapor compression cycles in which the temperature at each component inlet and outlet stays constant in steady-state. Table 4 represents the energy transfer in the regenerator, power input to the system and cooling and heating capacities of the system during one cycle in steady state. The values ①, ② and ③ show the energy transfer between magnetic field and MCM, between MCM and HTF and between HTF and the heat exchangers, respectively. Equations (14) and (15) represent the energies required to heat or cool MCM and HTF, respectively, due to the thermal capacitance of the component during cyclic heating and cooling. Because of these parasitic losses the COP of the AMRRC system significantly drops from 46.1 to 18.2. However, these losses can be decreased by optimizing the system. Figure 11 shows the temperature change of MCM during magnetization and demagnetization process and Figure 12 shows the temperature change of HTF during fluid flow process.

$$\text{Energy stored in MCM due to cyclic heating and cooling} = ① - ② = 12.4\text{kJ} \quad (14)$$

$$\text{Energy stored in HTF due to cyclic heating and cooling} = ② - ③ = 18.3\text{kJ} \quad (15)$$

Table 4: Energy transfer in regenerator, power input and cooling and heating capacity

① Magnetic E ↔ MCM (kJ)		② Heat transfer MCM ↔ HTF (kJ)		③ Heat transfer HTF → HX (kJ)		W_{input} (kJ)	$Q_{cooling}$ (kJ)	$Q_{heating}$ (kJ)
$Q_{ME\to MCM}$	$Q_{MCM\to ME}$	$Q_{MCM\to HTF}$	$Q_{HTF\to MCM}$	Q_h	Q_c			
51.8	50.7	39.4	38.3	21.1	20.0	1.10	0.70	1.80

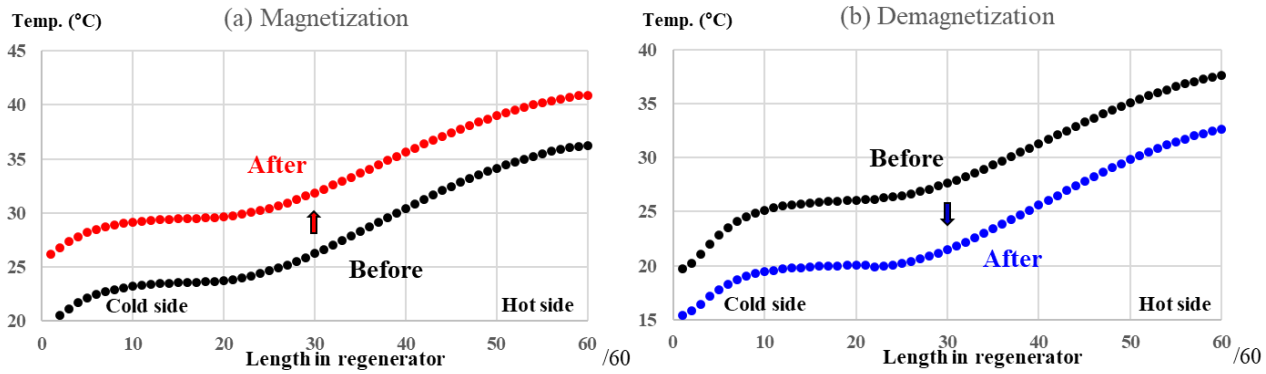

Figure 11: Temperature change of MCM during (a) magnetization and (b) demagnetization process

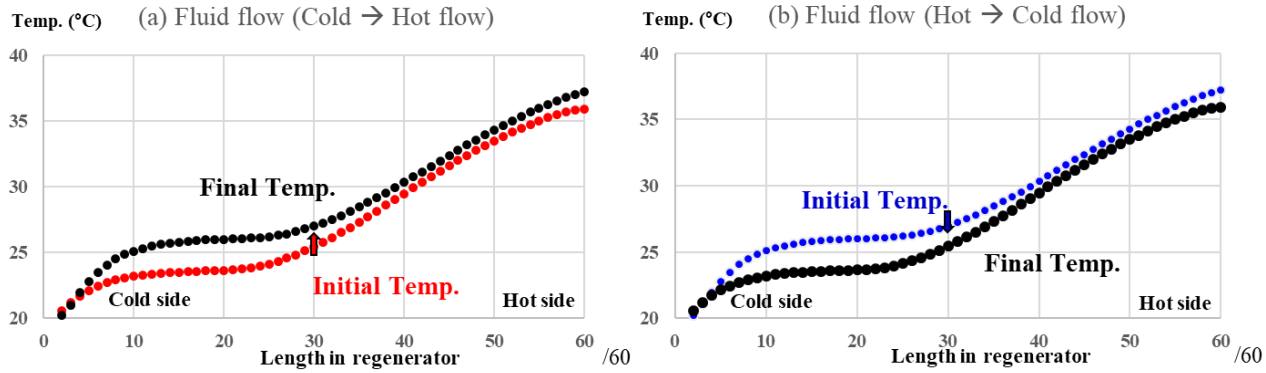

Figure 12: Temperature change of HTF during fluid flow (a) from cold to hot and (b) from hot to cold

3.5 Optimization of heat exchangers in AMRRC

In AMRRC system, the performance of the heat exchangers has impact on the performance of the system. If UA_c goes up, the cooling capacity will increase but the temperature of HTF returning to the regenerator on the cold side will

also increase, which causes a decrease in the system performance, and vice versa. Tables 5 and 6 show COP, $\dot{Q}_c$, $\dot{Q}_h$, $\dot{Q}_{cooling}$, $\dot{Q}_{heating}$, $T_{reservoir,hot}$, and $T_{reservoir,cold}$ as a function of UA_c and UA_h, respectively. According to Table 5, as UA_c goes up, the COP increases because of an increase in the cooling capacity. However, after UA_c reaches 2.9 kW/K, it has little effect on the performance of the system. According to Table 6, as UA_h goes down, the COP increases because of a decrease in heating capacity and $\dot{W}_{input}$. However, on the system level $\dot{W}_{input}$ increases after UA_h reaches 2.4 kW/K although the cooling capacity is same. This is because lower UA_h causes an increase in the temperature of the regenerator on the hot side, thereby increasing the heating capacity. On the system level, there is an optimum COP near UA_h of 2.4 kW/K.

Table 5: AMRRC performance results as a function of UA_c (after 2000 cycles)

UA_c (kW/K)	COP	$\dot{W}_{input}$ (kW)	$\dot{Q}_c$ (kW)	$\dot{Q}_h$ (kW)	$\dot{Q}_{cooling}$ (kW)	$\dot{Q}_{heating}$ (kW)	$T_{reservoir,hot}$ (°C)	$T_{reservoir,cold}$ (°C)
0.4	15.5	6.9	106.1	113.0	2.35	9.22	37.8	18.1
0.9	17.7	5.7	101.8	107.5	3.48	9.23	37.8	18.9
1.9	19.9	5.0	99.3	104.3	4.14	9.15	37.7	19.1
2.9	20.4	4.8	98.9	103.8	4.28	9.15	37.7	19.3
3.9	20.5	4.8	98.8	103.6	4.31	9.15	37.7	19.3
6.9	20.6	4.8	98.8	103.6	4.32	9.15	37.7	19.3
9.9	20.6	4.8	98.8	103.6	4.32	9.15	37.7	19.3
14.9	20.6	4.8	98.8	103.6	4.32	9.15	37.7	19.3

Table 6: AMRRC performance results as a function of UA_h (after 2000 cycles)

UA_h (kW/K)	COP	$\dot{W}_{input}$ (kW)	$\dot{Q}_c$ (kW)	$\dot{Q}_h$ (kW)	$\dot{Q}_{cooling}$ (kW)	$\dot{Q}_{heating}$ (kW)	$T_{reservoir,hot}$ (°C)	$T_{reservoir,cold}$ (°C)
1.4	17.7	5.7	101.8	107.5	3.48	9.23	37.8	18.9
2.4	15.8	5.4	86.1	91.6	3.48	8.96	35.1	18.9
3.4	14.7	5.5	81.1	86.6	3.48	9.01	34.3	18.9
4.4	14.2	5.5	78.7	84.3	3.48	9.05	33.9	18.9
9.4	13.5	5.6	75.6	81.2	3.48	9.12	33.4	18.9
14.4	13.4	5.6	75.2	80.8	3.48	9.13	33.3	18.9

6. CONCLUSIONS

This paper focuses on comparing different AMRRC models with and without heat transfer during the no flow period, which is a parasitic loss of the magnetic refrigeration cycle. It also investigates the effect of the energy required to heat or cool MCM and HTF due to the thermal capacitance of the component during cyclic heating and cooling on performance of the AMRRC system. A transient 1D model has been developed for these simulations. The model has also been used to optimize the heat exchangers of this particular AMRRC.

- It has been found that there is no significant difference in results between models with and without heat transfer during no flow period. The difference of heat transfer between these models is only 0.2 ~ 0.3 %.
- The COP of the AMRRC system significantly drops from 46.1 to 18.2 due to inherent parasitic losses by cyclic heating and cooling. However, these values can decrease by optimizing the AMRRC system.
- Under the conditions of Table 1, as the UA_c goes up, the COP and cooling capacity increase. However, beyond a UA_c of 2.9 kW/K, it has little effect on the performance of system. In addition, as UA_h goes down, the COP increases. However, there is an optimum COP near a UA_h of 2.4 kW/K on the system level.

NOMENCLATURE

The nomenclature should be located at the end of the text using the following format:

Nu	Nusselt number	(-)
Re	Reynolds number	(-)
Pr	Prandtl number	(-)

k	thermal conductivity	(W/m-K)
d_h	hydraulic diameter	(m)
a_s	specific surface area	(m^{-1})
A_c	cross-sectional area	(m^2)
T	temperature	(K)
$\dot{m}$	mass flow rate	(kg/s)
M	mass of reservoir tank	(kg)
c	specific heat capacity	(J/kg-K)
ρ	density	(kg/m^3)
$\dot{Q}$	heat transfer rate	(W)
$\dot{W}$	work rate	(W)
AMRRC	active magnetic regenerative refrigeration cycle	
MCM	magnetocaloric material	
HTF	heat transfer fluid	
COP	coefficient of performance	

Subscript

f	heat transfer fluid
mcm	magnetocaloric material
eff	effective conductivity
mag	magnetization
dem	demagnetization
i	initial
fi	final
res	reservoir tank

REFERENCES

Brown, J. S., & Domanski, P.A. (2014). Review of alternative cooling technologies. *Applied Thermal Engineering*, 64, 252–262.

Kitanovski, A., Tusek, J., Tomc, U., Plaznik, U., Ozbolt, M., & Poredos, A. (2014). Magnetocaloric energy conversion. New York: Springer

Steyert W. A. (1978). Stirling-cycle rotating magnetic refrigerators and heat engines for use near room temperature. *J Appl Phys*, 49, 1216–1226

Barclay J. A., Steyert W. A. (1982). Active magnetic regenerator. US Patent No 4.332.135

Engelbrecht, K. (2004). *A numerical model of an active magnetic regenerator refrigeration system* (Masters dissertation). The University of Wisconsin-Madison.

Peterson, T. F., Pryds, N., Smith, A., Hattel, J., Schmidt, H, & Knuden, H. H. (2008). Two-dimensional mathematical model of a reciprocating room-temperature active magnetic regenerator. *Int. J. Refrig.*, 31, 432-443.

Tishin, A. M., Gschneidner, K. A., & Percharsky, V. K. (1999). Magnetocaloric effect and heat capacity in the phase-transition region. *Physical review B*, 59(1), 503-511

Aprea, C., Greco, A., & Maiorino, A. (2013). The use of the first and of the second order phase magnetic transition alloys for an AMR refrigerator at room temperature: Anumerical analysis of the energy performances. *Energy Conversion and Management*, 70, 40-55.

Dixon, A. G., & Cresswell, D. L. (1979). Theoretical predictions of effective heat transfer mechanisms in regular shaped packed beds. *AIChE Journal*, 25, 663–676.

Wakao, N., & Kaguei, S. (1982) Heat and Mass Transfer in Packed Beds, New York: Gordon and Breach.

Engelbrecht, K. (2008). *A numerical model of an active regenerator refrigerator with experimental validation* (Doctoral dissertation). The University of Wisconsin-Madison.

ACKNOWLEDGEMENT

The authors would like to thank the member companies of the Air Conditioning and Refrigeration Center at the University of Illinois at Urbana-Champaign for their support.